JACS
JOURNAL OF THE AMERICAN CHEMICAL SOCIETY
Article
pubs.acs.org/JACS

# Toward Inexpensive Superhard Materials: Tungsten Tetraboride-Based Solid Solutions

Reza Mohammadi,[†,‡] Miao Xie,[†] Andrew T. Lech,[†] Christopher L. Turner,[†] Abby Kavner,[§] Sarah H. Tolbert,*[,†,‡,⊥] and Richard B. Kaner*[,†,‡,⊥]

[†]Department of Chemistry and Biochemistry, [‡]Department of Materials Science and Engineering, and [§]Department of Earth and Space Sciences, University of California, Los Angeles, Los Angeles, California, United States

[⊥]California NanoSystems Institute (CNSI), University of California, Los Angeles, Los Angeles, California, United States

Supporting Information

**ABSTRACT:** To enhance the hardness of tungsten tetraboride ($WB_4$), a notable lower cost member of the late transition-metal borides, we have synthesized and characterized solid solutions of this material with tantalum (Ta), manganese (Mn), and chromium (Cr). Various concentrations of these transition-metal elements, ranging from 0.0 to 50.0 at. %, on a metals basis, were made. Arc melting was used to synthesize these refractory compounds from the pure elements. Elemental and phase purity of the samples were examined using energy-dispersive X-ray spectroscopy (EDS) and X-ray diffraction (XRD), and microindentation was utilized to measure the Vickers hardness under applied loads of 0.49−4.9 N. XRD results indicate that the solubility limit is below 10 at. % for Cr and below 20 at. % for Mn, while Ta is soluble in $WB_4$ above 20 at. %. Optimized Vickers hardness values of 52.8 ± 2.2, 53.7 ± 1.8, and 53.5 ± 1.9 GPa were achieved, under an applied load of 0.49 N, when ∼2.0, 4.0, and 10.0 at. % Ta, Mn, and Cr were added to $WB_4$ on a metals basis, respectively. Motivated by these results, ternary solid solutions of $WB_4$ were produced, keeping the concentration of Ta in $WB_4$ fixed at 2.0 at. % and varying the concentration of Mn or Cr. This led to hardness values of 55.8 ± 2.3 and 57.3 ± 1.9 GPa (under a load of 0.49 N) for the combinations $W_{0.94}Ta_{0.02}Mn_{0.04}B_4$ and $W_{0.93}Ta_{0.02}Cr_{0.05}B_4$, respectively. *In situ* high-pressure XRD measurements collected up to ∼65 GPa generated a bulk modulus of 335 ± 3 GPa for the hardest $WB_4$ solid solution, $W_{0.93}Ta_{0.02}Cr_{0.05}B_4$, and showed suppression of a pressure-induced phase transition previously observed in pure $WB_4$.

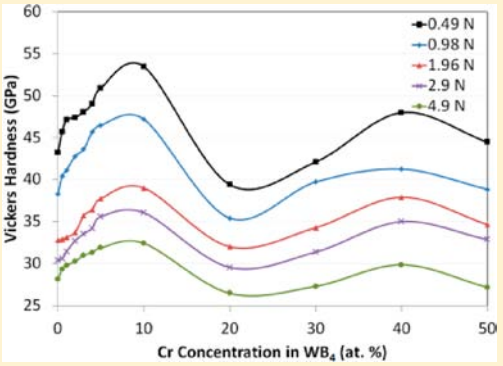


## INTRODUCTION

The concept of creating superhard materials by introducing boron into the structure of dense transition metals is now well established.[1−3] Rhenium diboride ($ReB_2$) is one successful example of such compounds, which are potential candidates to replace expensive ultrahard materials, such as diamond and cubic boron nitride (*c*-BN), in a wide range of applications from cutting tools to wear protecting surfaces. With a Vickers microindentation hardness greater than 40 GPa (under an applied load of 0.49 N), $ReB_2$ has demonstrated very interesting properties, such as facile synthesis at ambient pressure,[4] high electrical conductivity,[5] and excellent elastic moduli.[6−8]

Since the short covalent boron−boron bonds have been found to play a significant role in the high hardness of dense transition-metal borides,[2,9,10] one might expect that harder materials could be created by increasing the boron concentration in the structure, which should result in an increased number of boron−boron bonds. Besides making harder materials, substituting some atoms of the less-expensive boron for the more expensive transition metal could reduce the ultimate cost of production for applications such as high-performance cutting tools. Over the past few years, this strategy has led to a great deal of pioneering research on superhard materials based on high boron content transition-metal borides, with tungsten tetraboride ($WB_4$) being a prime example.[11−14]

The possibility that $WB_4$ could possess a high hardness was first explored by Brazhkin et al. in 2002,[15] and we discussed its potential applications as a superhard material in 2005.[1] Then, Gu et al.[16] reported hardness values of 46.0 and 31.8 GPa (under applied loads of 0.49 and 4.9 N, respectively), but the work did not describe the synthetic methods used or give details on phase purity. Recently, we systematically investigated the mechanical properties of $WB_4$.[17,18] Tungsten tetraboride was synthesized by arc melting at ambient pressure, and its mechanical properties were characterized using microindentation, nanoindentation and *in situ* high-pressure X-ray diffraction (XRD). A bulk modulus of 326−339 GPa, Vickers microindentation hardness (under a load of 0.49 N) of 43.3 GPa and nanoindentation hardness (at a penetration depth of 250 nm) of 40.4 GPa were measured using *in situ* high-pressure XRD, microindentation, and nanoindentation, respectively. Applying a high hydrostatic pressure of ∼40 GPa, this material

**Received:** August 18, 2012
**Published:** November 21, 2012

   dx.doi.org/10.1021/ja308219r | *J. Am. Chem. Soc.* 2012, 134, 20660−20668

underwent a unique reversible second-order phase transition that was attributed to its rigid structure.[18]

In an attempt to further increase the hardness of $WB_4$, we added rhenium (Re) at different concentrations on a metals basis. By increasing the Re concentration from 0.0 to 50.0 at. %, the low-load hardness (under 0.49 N) increased from 43.3 GPa for pure $WB_4$ to a maximum value of 49.8 GPa for 1 at. % Re and then decreased to a minimum value of about 29 GPa for 20 at. % Re, followed by an increase to about 34 GPa for 50 at. % Re addition. Similar trends were observed for the hardness changes under other loads (0.98, 1.96, 2.94, and 4.9 N). This hardness behavior was attributed to the formation of an $ReB_2$ second phase that appears at ∼0.5 at. % Re, resulting in dispersion hardening, which is most effective at ∼1 at. % Re.[17]

In addition to dispersion hardening, which contributes an extrinsic component to the hardness and other mechanical properties, there are some other dislocation-pinning mechanisms that may be used to enhance the hardness of a material if designed properly. These mechanisms include solid solution hardening, grain boundary strengthening, precipitation hardening, and strain hardening. Among these, solid solution hardening is one of the most efficient ways to increase the hardness of a material without introducing a second phase.[19] Solid solutions are established as an effective way to tune the hardness of transition-metal borides, as previously observed for several compounds, including ruthenium diboride ($RuB_2$) when it forms solid solutions with osmium (Os).[20] A full range of solid solutions containing Os substituted for Ru in $RuB_2$ can be produced and they show a low-load hardness that increases linearly from ∼21 to 28 GPa.

To explore enhancements to the hardness of $WB_4$, here we add tantalum (Ta), manganese (Mn), and chromium (Cr) to form solid solutions. The resulting structural and hardness changes are reported along with an examination of possible mechanisms to explain the changes that include electronic structure changes, solid solution hardening, and dispersion hardening. As an additional step, we tried to create even harder $WB_4$ solid solutions by superimposing the hardening effects of elements with different atomic size and valence electron count to further intensify either dislocation-locking mechanism or electronic structure changes. We specifically examined elements with atomic radii both larger (Ta = 1.49 Å) and smaller (Mn = 1.32 or Cr = 1.30 Å) than tungsten (W = 1.41 Å; note B = 0.78 Å), and with valence electron counts both larger (Mn, Group VII) and smaller (Ta, Group V) than tungsten (W and Cr, Group VI).[21] The bulk modulus, high-pressure stability, and thermal stability of the hardest solid solution are also reported and compared directly to $WB_4$.

## EXPERIMENTAL PROCEDURE

High-purity powders of tungsten (99.95%, Strem Chemicals, U.S.A.), amorphous boron (99+%, Strem Chemicals, U.S.A.), tantalum (99.9%, ROC/RIC Corp., U.S.A.), manganese (99.9%, Fisher Scientific Co., U.S.A.), and chromium (99.9%, ROC/RIC Corp., U.S.A.) were used to systematically study the effect of compositional variations on the hardness of $WB_4$. The powders at each desired set of compositions, i.e., $W_{1-x}Ta_xB_4$, $W_{1-x}Mn_xB_4$, and $W_{1-x}Cr_xB_4$ ($x$ = 0.0–0.5), were ground together thoroughly in an agate mortar and pestle in order to obtain relatively homogeneous mixtures. While keeping the molar ratio of W:B in all mixtures constant at 1:12, different concentrations of tantalum, manganese, and chromium in $WB_4$ were made, on a metals basis, in an attempt to make solid solutions with increased hardness. Note that excess boron is required for the synthesis in order to stop the formation of soft thermodynamically favorable impurity phases, such as tungsten diboride ($WB_2$).[11,12,17]

Each powder mixture was pressed into a ∼300 mg pellet using a hydraulic (Carver) press under an applied load of ∼10 000 lbs. The pellets were then arc-melted, under high-purity argon at ambient pressure, by applying an ac current of ∼70 amps for ∼5 min. The as-synthesized ingots were cut in half using a sinter-bonded diamond lapidary sectioning saw (South Bay Technology Inc., U.S.A.). One half of the ingot was crushed, using a hardened steel mortar and pestle set, into a very fine powder for XRD experiments and thermal gravimetric analysis. The other half was mounted in epoxy using a cold-mount resin/hardener epoxy set (Allied High Tech Products Inc., U.S.A.). The epoxy mounted sample was then polished with a tripod polisher (South Bay Technology Inc., U.S.A.), using polishing papers of grit sizes ranging from 120 to 1200 (Allied High Tech Products Inc., U.S.A.) followed by diamond abrasive films containing diamond particles ranging from 30 to 0.5 $\mu$m (South Bay Technology Inc., U.S.A.), to achieve an optically flat surface for elemental analysis and hardness testing.

To check the elemental and phase purity of the samples, energy-dispersive X-ray spectroscopy (EDS) and XRD were used. The optically flat mounted samples were examined for elemental composition and purity utilizing an EDAX detector mounted on a scanning electron microscope (JEOL JSM 6700 F, Japan). The phase identification was carried out on the crushed powder samples using an X'Pert Pro powder X-ray diffraction system (PANalytical, Netherlands). Using a Cu K$\alpha$ X-ray beam ($\lambda$ = 1.5418 Å), XRD patterns were collected from the powder samples using the following parameters: step size = 0.03°, time per step =100.00 s, and scan speed = 0.0425 °/s. The patterns were then compared to reference patterns available in the Joint Committee on Powder Diffraction Standards (JCPDS) database to determine the phases present in the samples.

After the purity and composition of the arc-melted ingots were tested, the hardness of each polished sample was measured using a MicroMet 2103 microhardness tester (Buehler Ltd., U.S.A.) equipped with a pyramid diamond indenter tip. With a dwell time of 15 s, the samples were indented using five different applied loads of 0.49 (low load), 0.98, 1.96, 2.94, and 4.9 N (high load). The lengths of the diagonals of the impression marks, created by the indenter on the surface of the samples, were then measured using a high-resolution Zeiss Axiotech 100HD optical microscope (Carl Zeiss Vision GmbH, Germany) under a total magnification of 500×. The Vickers microindentation hardness values ($H_v$, in GPa), under various applied loads, were calculated using eq 1:

$$H_v = 1854.4P/d^2 \quad (1)$$

where $P$ is the applied load in Newtons (N) and $d$ is the arithmetic mean of the diagonals of the indent in micrometers ($\mu$m). Each hardness datum point reported here represents the average of the indentation measurements for at least 20 randomly chosen spots on the sample at each load to ensure accurate results. The standard deviations of the mean hardness values under the applied loads of 0.49, 0.98, 1.96, 2.94, and 4.9 N are respectively within 5.60, 4.11, 3.68, 2.84, and 1.57 GPa.

The lattice elastic compressibility of the hardest phase, i.e., $W_{0.93}Ta_{0.02}Cr_{0.05}B_4$, was measured using synchrotron-based *in situ* high-pressure XRD in a Diacell diamond anvil cell. To ensure a quasihydrostatic sample environment, neon gas was loaded into the cell using the Consortium for Materials Properties Research in Earth Sciences (COMPRES) and GeoSoilEnviroCARS (GSECARS) gas loading system.[22] Diffraction patterns were collected for the powder samples from ambient pressure to ∼65 GPa on Beamline 12.2.2 at the Advanced Light Source at Lawrence Berkeley National Laboratory (LBNL, CA, U.S.A.) with X-ray beam size of approximately 10 × 10 $\mu$m.[18] The pressure–volume data, measured by XRD, were fit using the third-order finite strain Birch–Murnaghan equation of state (eq 2) to infer the room-pressure isothermal bulk modulus ($K_{0T}$) and its first derivative with respect to pressure ($K_{0T}'$). The third-order equation


dx.doi.org/10.1021/ja308219r | J. Am. Chem. Soc. 2012, 134, 20660–20668

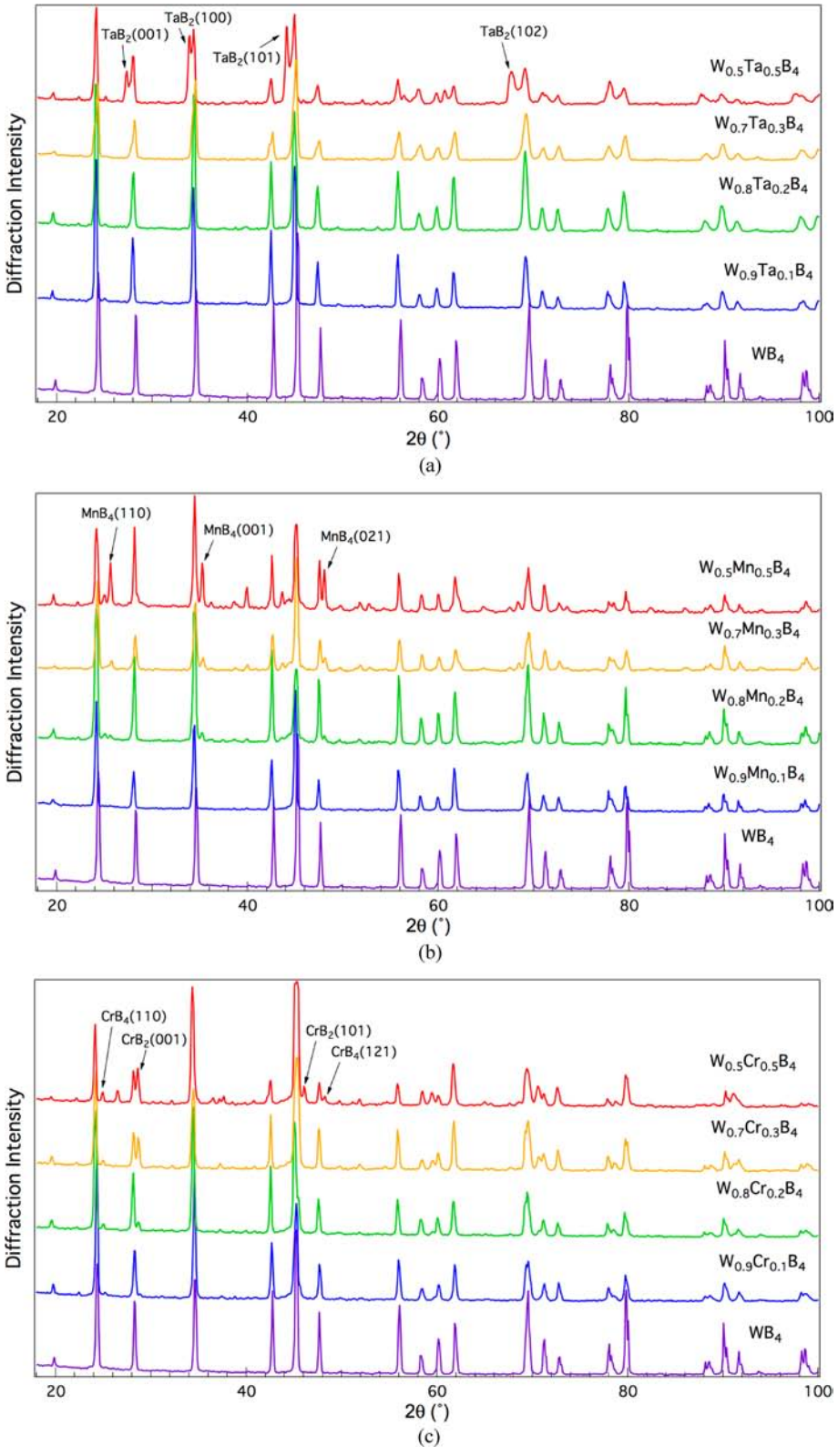


**Figure 1.** XRD patterns of $WB_4$ when 0−50 at. % tantalum (a), manganese (b), and chromium (c) are added on a metals basis. The bottom pattern in each figure belongs to pure $WB_4$ (JCPDS ref code: 00-019-1373). Note that the solubility limit is less than 10 at. % for Cr and below 20 at. % for Mn, while the solubility of Ta in $WB_4$ is greater than 20 at. %. Above 20 at. % Ta, $TaB_2$ (JCPDS ref code: 03-065-3385) and at and above 20 at. % Mn and 10 at. % Cr, $MnB_4$ (JCPDS ref code: 03-065-6232) and a mixture of $CrB_2$ and $CrB_4$ (JCPDS ref codes: 00-022-0208 and 00-034-0369) appear respectively in the patterns as second phases (shown by arrows). To give the reader a clearer picture, only six patterns (0, 10, 20, 30, 40, and 50 at. % of Ta, Mn, and Cr), which are most useful to follow the structural changes, have been chosen in each series and displayed herein at higher magnification.


dx.doi.org/10.1021/ja308219r | J. Am. Chem. Soc. 2012, 134, 20660−20668

Table 1. Lattice Parameters and Selected *d*-Spacings for $WB_4$ and Some of Its Hardest Solid Solutions[a]

| compound | $a$ (Å) | $c$ (Å) | $V$ (Å$^3$) | $d_{100}$ (Å) | $d_{101}$ (Å) | $d_{002}$ (Å) | $d_{110}$ (Å) | $d_{112}$ (Å) |
|---|---|---|---|---|---|---|---|---|
| $WB_4$ | 5.199(8) | 6.338(4) | 148.4 | 4.50316 | 3.67101 | 3.16920 | 2.59990 | 2.01006 |
| $W_{0.98}Ta_{0.02}B_4$ | 5.200(5) | 6.341(2) | 148.5 | 4.50375 | 3.67186 | 3.17057 | 2.60024 | 2.01057 |
| $W_{0.80}Ta_{0.20}B_4$ | 5.206(4) | 6.356(5) | 149.2 | 4.50876 | 3.67738 | 3.17781 | 2.60313 | 2.01375 |
| $W_{0.96}Mn_{0.04}B_4$ | 5.200(2) | 6.341(4) | 148.5 | 4.50348 | 3.67174 | 3.17063 | 2.60009 | 2.01051 |
| $W_{0.90}Cr_{0.10}B_4$ | 5.200(2) | 6.340(6) | 148.5 | 4.50348 | 3.67161 | 3.17029 | 2.60009 | 2.01042 |
| $W_{0.96}Ta_{0.02}Mn_{0.02}B_4$ | 5.199(4) | 6.339(1) | 148.4 | 4.50286 | 3.67097 | 3.16953 | 2.59973 | 2.01006 |
| $W_{0.88}Ta_{0.02}Mn_{0.10}B_4$ | 5.199(3) | 6.338(1) | 148.4 | 4.50276 | 3.67072 | 3.16901 | 2.59967 | 2.0099 |
| $W_{0.96}Ta_{0.02}Cr_{0.02}B_4$ | 5.199(1) | 6.337(7) | 148.4 | 4.50254 | 3.67053 | 3.16883 | 2.59954 | 2.0098 |
| $W_{0.93}Ta_{0.02}Cr_{0.05}B_4$ | 5.199(4) | 6.333(5) | 148.3 | 4.50278 | 3.66983 | 3.16671 | 2.59968 | 2.00932 |
| $W_{0.88}Ta_{0.02}Cr_{0.10}B_4$ | 5.199(7) | 6.336(5) | 148.4 | 4.50309 | 3.6706 | 3.16824 | 2.59986 | 2.0098 |

[a]Measured using powder XRD. Error values are quoted in parentheses.

shown below reduces to the second-order equation when $K_{0T}'$ is equal to 4.

$$P = (3/2)K_0[(V/V_0)^{-7/3} - (V/V_0)^{-5/3}]\{1 - (3/4)(4 - K_0')[(V/V_0)^{-2/3} - 1]\} \quad (2)$$

To investigate the thermal stability of the hardest solid solution, a Pyris Diamond thermogravimetric/differential thermal analyzer module (TG-DTA, Perkin-Elmer Instruments, U.S.A.) was utilized. Powder samples were heated in air up to 200 °C at a rate of 20 °C/min and held at this temperature for 20 min to remove any moisture. The samples were then heated up to 1000 °C at a rate of 2 °C/min and soaked at this temperature for 120 min. The samples were next air cooled to room temperature at a rate of 5 °C/min. XRD was performed on the samples after the thermal analysis experiments to identify the resulting phase(s).

## RESULTS AND DISCUSSION

EDS was used to verify the elemental purity and composition of the samples. The EDS results confirmed the desired atomic ratios of elements as well as the absence of any impurity elements in the samples. The phase purity and composition of the samples were then checked using powder XRD. The XRD patterns for the compounds $W_xTa_{1-x}B_4$, $W_xMn_{1-x}B_4$ and $W_xCr_{1-x}B_4$ ($x$ = 0.0−0.5) are shown in Figure 1a−c, respectively. Note that all samples contain some excess crystalline boron, which is unobservable using standard XRD at low scan times.

Figure 1a displays the XRD patterns of the tantalum-added compounds, $W_xTa_{1-x}B_4$. These patterns show that the solubility of Ta in $WB_4$ (the bottom pattern) is greater than 20 at. %, above which point $TaB_2$ appears as a second phase (JCPDS ref code: 03-065-3385). The patterns of manganese-added compounds, $W_xMn_{1-x}B_4$, are shown in Figure 1b. The solubility of manganese in $WB_4$ is below 20 at. %. At and above 20 at. % Mn addition, $MnB_4$ starts to show up as an impurity phase (JCPDS ref code: 03-065-6232). Chromium has the largest size difference compared to tungsten, and in agreement with this fact, the solubility of chromium in $WB_4$ appears to be less than 10 at. %, as can be seen in Figure 1c. At and above 10 at. % Cr, two phases corresponding to $CrB_2$ and $CrB_4$ (with JCPDS ref codes of 00-034-0369 and 00-022-0208, respectively) start appearing simultaneously. It should be noted that because of the rapid cooling times involved in the arc melting process, it is not possible to determine if the formation of second phases in these three series is the result of kinetic competition among the various transition-metal borides or an actual thermodynamic solubility limit.

The lattice parameters of the hardest $WB_4$ solid solutions are given in Table 1. It can be concluded from the data in this table that the addition of small amounts of Ta, Mn, and Cr does not change the lattice parameters of $WB_4$, within the error of the measurement. Larger quantities of these elements, however, can influence the lattice parameters of $WB_4$, as is observed in $W_{0.8}Ta_{0.2}B_4$, for example; the change is due to the atomic size mismatch between tungsten and these three elements.

Once the purity and composition of the samples were verified using EDS and XRD, the Vickers hardness of each of the samples, under different applied loads ranging from 0.49 to 4.9 N, were measured using microindentation, as shown in Figure 2a−c. Figure 2a shows that the hardness, under an applied load of 0.49 N (low load), increases from 43.3 ± 2.9 GPa for pure $WB_4$ ($x$ = 0.0) to a maximum of 52.8 ± 2.2 GPa with the addition of 2 at. % Ta. The hardness then decreases to 43.7 ± 2.1 GPa for 5 at. % Ta followed by a broad peak between 10 and 20 at. % at about 44 GPa. Once the solubility limit is significantly exceeded, the hardness rises slightly, showing a value of 44.6 ± 3.7 GPa for a Ta concentration of 40 at. %. It is likely that the broad peak in hardness at high concentration in the two phase system stems from a fundamentally different mechanism than the hardness peak at low concentration. Similar trends are observed for the hardness under each of the other loads tested (0.98, 1.96, 2.94, and 4.9 N).

For the $WB_4$−Mn system (Figure 2b), the trends in the Vickers hardness show some similarities to the $WB_4$−Ta data. At low load (0.49 N), these data again show a peak in the hardness at a low Mn concentration (53.7 ± 1.8 GPa with the addition of 4 at. % Mn). This is followed by a decreases in hardness to 46.9 ± 3.8 GPa at 5 at. % Mn addition. In contrast to Ta, Mn shows a second significant peak in the low load data between 10 and 20 at. % at ∼55 GPa. Higher loads show more of a plateau in this range, similar to the Ta data. Again, similar to the trends observed upon Ta addition, the data show a final broad hump between 30 and 40 at. % Mn addition, in the range where the sample contains a two phase mixture.

The addition of Cr to $WB_4$ (Figure 2c) shows trends intermediate between Ta and Mn. Only two peaks are observed in the plot of hardness as a function of Cr concentration, but the first peak is at higher Cr content than that observed for Ta or Mn. For example, addition of 10 at. % Cr on a metals basis results in an increase in hardness (at 0.49 N) from 43.3 ± 2.9 GPa for pure $WB_4$ to 53.5 ± 1.9 GPa. As with the other samples, a second peak in hardness is observed for Cr concentrations above the solubility limit. After dropping


dx.doi.org/10.1021/ja308219r | J. Am. Chem. Soc. 2012, 134, 20660−20668

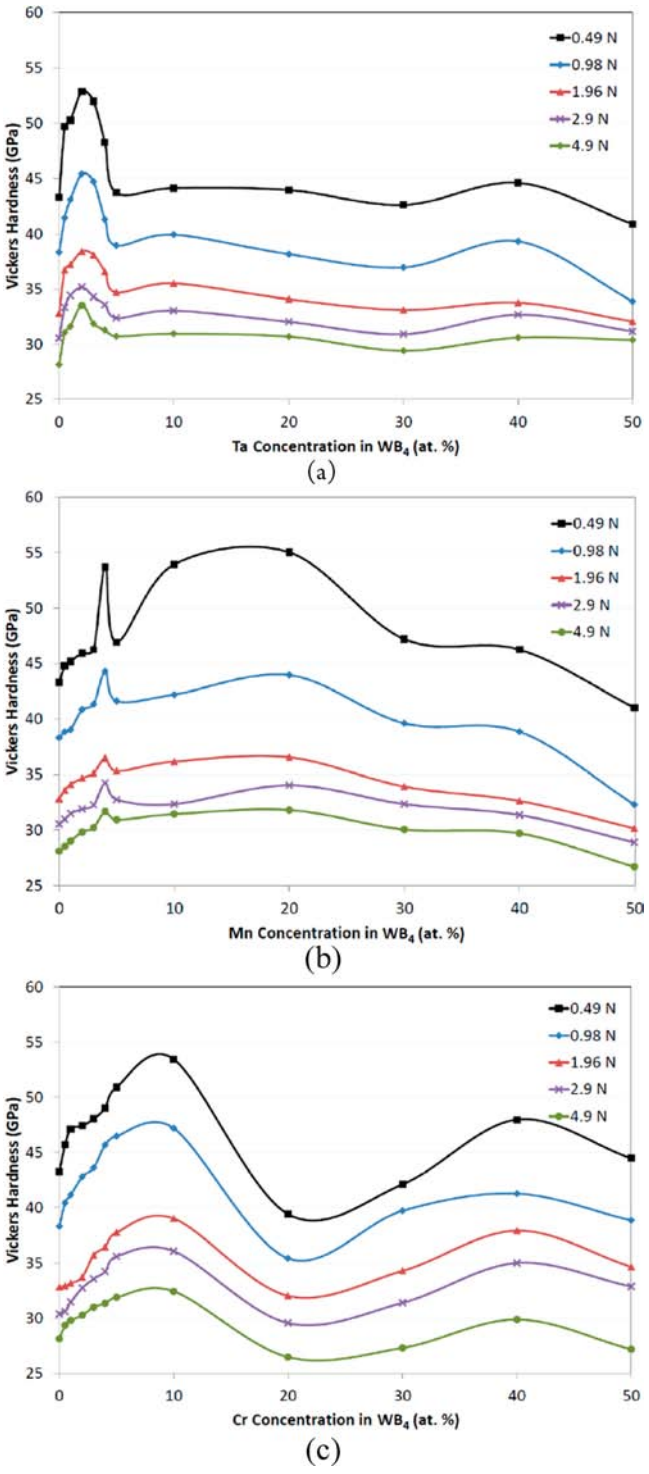


**Figure 2.** Vickers microindentation hardness of tungsten tetraboride solid solutions with Ta (a), Mn (b), and Cr (c) under loads ranging from 0.49 to 4.9 N (low to high loads, respectively). The concentrations were varied in $WB_4$ by adding 0–50 at. % Ta, Mn, and Cr on a metals basis (see Figure 1).

down to 39.4 ± 5.6 GPa at ~20 at. % Cr, the hardness again increases to 48.0 ± 5.2 GPa at a concentration of 40 at. % Cr.

Although the actual structure of $WB_4$ is subject to debate, there is a general agreement among all the models proposed so far that the structure of this superhard material consists of alternating hexagonal layers of boron and tungsten, with some of the tungsten atoms missing.[11,16−18,23,24] Since our EDS area mapping analyses along with XRD results (Figure 1 and Table 1) precludes the possibility of grain boundary strengthening mechanisms within the solubility limits of these three elements (Ta, Mn and Cr) in $WB_4$, we therefore postulate that the defect structure of this material may be responsible for the hardening trends observed for the solid solutions in Figure 2a–c. Located in different Groups of the Periodic Table, tantalum (Group V) and manganese (Group VII) each have a different number of valence electrons than tungsten (Group VI). At low concentrations, by sitting at the positions of missing tungsten atoms, these elements could induce either tungsten vacancies (by adding Mn) or boron vacancies (by adding Ta) to the $WB_4$ structure.

These ideas are supported by recent calculations by Gou et al. who examined the electronic and mechanical properties of defective tungsten borides by first-principle calculations.[24] They found that the presence of vacancies in the $WB_4$ structure is not only energetically favored, because of the significant decrease in the heat of formations compared to the vacancy-free borides, but is also electronically preferred due to the substantial reduction of the Fermi level. In addition, their calculations show that the shear modulus, which is directly related to hardness,[25] of $WB_4$ demonstrates an increase in the presence of both tungsten and boron vacancies. These valence electron differences, together with the atomic size mismatches (Ta = 1.49, Mn = 1.32, and W = 1.41 Å),[21] might explain the first hardness increase for $WB_4$ solid solutions with Ta and Mn at concentrations of 2 and 4 at. %, on a metals basis, respectively.

The addition of Cr, which is in the same Group as tungsten in the Periodic Table (Group VI), to the $WB_4$ structure would not generate vacancies. As a result, for Cr solid solutions with $WB_4$ the hardness increase at low concentrations is expected to be due only to the atomic size difference (Cr = 1.30 Å). This fact may explain the lack of a distinct peak at very low concentrations for the Cr/W solid solutions.

After filling some of the missing tungsten positions by the atoms of each of these three elements at low concentrations, they likely start replacing tungsten atoms in other positions, as the concentration increases. This could result in classical solid solution hardening, driven exclusively by atomic-size mismatch. This would correspond to the second hardness increase at a maximum solubility of ~20 at. % for Ta and Mn additions on a metals basis as well as the first hardness increase at ~10 at. % for Cr. The observation that this peak is most significant for Cr is well justified by the fact that the size mismatch between W and Cr is greater than the mismatch between W and Mn or Ta. The third peak in the hardness data of Ta (~40 at. % in Figure 2a) and Mn (~40 at. % in Figure 2b) and the second one of Cr (~40 at. % in Figure 2c) in $WB_4$ may be attributed to dispersion hardening, which is an extrinsic effect due to the presence of a second phase (i.e., $TaB_2$, $MnB_4$, and $CrB_2$ + $CrB_4$ in $WB_4$).[17,26] Clear diffraction peaks from these second phases can be seen in Figure 1a–c.

These results motivated us to run a series of experiments in which the concentration of Ta in $WB_4$ was kept constant at 2 at. % on a metals basis and those of Mn or Cr were varied from 2 to 10 at. %, in an effort to combine both electronic structure and solution hardening effects. The XRD and hardness data obtained for these compounds are shown in Figure S1 and Tables 2–3, respectively. The XRD results (Figure S1 and Table 1) confirm that in the presence of 2 at. % Ta, the solubility of both Mn and Cr in $WB_4$ is limited to less than 10 at. %. Note from Table 1, however, that the lattice parameters


dx.doi.org/10.1021/ja308219r | J. Am. Chem. Soc. 2012, 134, 20660–20668

**Table 2. Vickers Microindentation Hardness Data for $W_{0.98-x}Ta_{0.02}Mn_xB_4$ Solid Solutions, with $x$ = 0.02−0.1, under Applied Loads Ranging From 0.49−4.9 N**

| | applied load (N) | | | | |
|---|---|---|---|---|---|
| compound | 0.49 | 0.98 | 1.96 | 2.94 | 4.9 |
| $WB_4$ | 43.3 | 38.3 | 32.8 | 30.5 | 28.1 |
| $W_{0.96}Ta_{0.02}Mn_{0.02}B_4$ | 49.6 | 45.4 | 34.3 | 33.3 | 29.5 |
| $W_{0.94}Ta_{0.02}Mn_{0.04}B_4$ | 55.8 | 46.7 | 37.0 | 34.8 | 30.9 |
| $W_{0.88}Ta_{0.02}Mn_{0.10}B_4$ | 47.2 | 36.9 | 33.1 | 31.5 | 30.4 |

**Table 3. Vickers Microindentation Hardness Data for $W_{0.98-x}Ta_{0.02}Cr_xB_4$ Solid Solutions, with $x$ = 0.02−0.1, under Applied Loads Ranging From 0.49−4.9 N[a]**

| | applied load (N) | | | | |
|---|---|---|---|---|---|
| compound | 0.49 | 0.98 | 1.96 | 2.94 | 4.9 |
| $WB_4$ | 43.3 | 38.3 | 32.8 | 30.5 | 28.1 |
| $W_{0.96}Ta_{0.02}Cr_{0.02}B_4$ | 46.2 | 39.6 | 33.1 | 31.5 | 29.0 |
| $W_{0.93}Ta_{0.02}Cr_{0.05}B_4$ | 57.3 | 44.1 | 38.2 | 34.8 | 31.7 |
| $W_{0.88}Ta_{0.02}Cr_{0.10}B_4$ | 49.9 | 43.0 | 37.8 | 34.5 | 30.8 |

[a]Highest hardness of 57.3 GPa (at 0.49 N) was measured for the $W_{0.93}Ta_{0.02}Cr_{0.05}B_4$ solid solution.

remain almost unchanged, considering the error values, when Ta and Mn or Cr are simultaneously added to $WB_4$. As can be seen in Tables 2 and 3, the highest hardness values of 55.8 ± 2.3 and 57.3 ± 1.9 GPa (under a load of 0.49 N) are achieved for the concentrations $W_{0.94}Ta_{0.02}Mn_{0.04}B_4$ (Table 2) and $W_{0.93}Ta_{0.02}Cr_{0.05}B_4$ (Table 3), respectively. This hardness increase, which is also observed under other hardness loads, is likely due to the combined effects of introducing charges (by Ta and Mn), and thus vacancies, to the structure of $WB_4$ and atomic size mismatches. Since the superposition of electronic charges imposed on the structure of $WB_4$ by adding 2 at. % Ta and 4 at. % Mn (in $W_{0.94}Ta_{0.02}Mn_{0.04}B_4$) is the same as that of adding 2 at. % Ta and 5 at. % Cr (in $W_{0.93}Ta_{0.02}Cr_{0.05}B_4$) but of opposite signs, these two compounds should contain similar amounts of vacancies although of different types (tungsten and boron, respectively). This could result in similar hardness values; however, the smaller size of Cr ($r$ = 1.30 Å) compared to Mn ($r$ = 1.32 Å)[21] along with the higher Cr concentration might be the reason for the slightly higher hardness of the $W_{0.93}Ta_{0.02}Cr_{0.05}B_4$ (57.3 GPa) solid solution in comparison to $W_{0.94}Ta_{0.02}Mn_{0.04}B_4$ (55.8 GPa). Note that the highest hardness value of 57.3 GPa, measured for the $W_{0.93}Ta_{0.02}Cr_{0.05}B_4$ solid solution, is respectively ∼16 and 24% higher than those of $ReB_2$ (48.0 GPa)[4] and $WB_4$ (43.3 GPa),[17] the hardest transition-metal borides reported to date.

Superhard materials generally possess a high bulk modulus;[2,4,17,18] thus, the measured lattice volume as a function of pressure was used to determine the bulk modulus of $W_{0.93}Ta_{0.02}Cr_{0.05}B_4$, the solid solution showing the highest hardness. A series of representative diffraction patterns for this solid solution is shown in Figure S2. The data were collected up to 65 GPa and were fit both over the full pressure range and over only the range from 0−40 GPa (Figure 3a). The latter fitting was done for a fair comparison with pure $WB_4$, which undergoes a second-order phase transition at ∼40 GPa. The fit of the data up to 40 GPa resulted in an isothermal bulk modulus of $K_{0T}$ = 366 ± 14 GPa with $K_{0T}'$ = 2.6 ± 0.9. The bulk modulus and its first derivative are not independent parameters, and the bulk modulus is equal to 346 ± 3 GPa

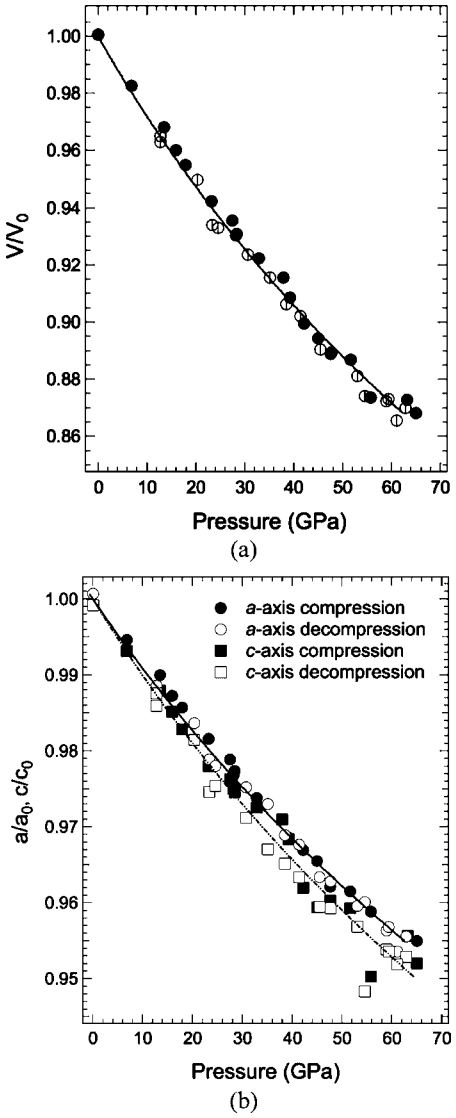


**Figure 3.** Measured fractional unit cell volume (a) and fractional lattice parameters (b) of the hardest $WB_4$ solid solution, i.e., $W_{0.93}Ta_{0.02}Cr_{0.05}B_4$, plotted as a function of pressure. The data were collected using *in situ* high-pressure XRD up to 65 GPa. All the lines are Birch−Murnaghan fit to the data. Fitting the compression data to a second-order Birch−Murnaghan equation of state resulted in a zero-pressure bulk modulus of 335 GPa when its derivative with respect to pressure was set to 4. The close linear compressibilities of the *a*- and *c*-axes indicate a mechanically more isotropic structure for the hardest solid solution when compared to pure $WB_4$. Error bars are within the size of the symbols.

when $K_{0T}'$ is set equal to 4. These values are comparable to the corresponding values for $WB_4$, determined using the same pressure range: $K_{0T}$ = 369 ± 9 GPa with $K_{0T}'$ = 1.2 ± 0.5 and $K_{0T}$ =326 ± 3 GPa with $dK_{0T}/dP$ set equal to 4.[17,18] Unlike $WB_4$, $W_{0.93}Ta_{0.02}Cr_{0.05}B_4$ shows no signs of a lattice instability at 40 GPa. Slightly lower values of the bulk modulus were obtained over the pressure range of 0−65 GPa with $K_{0T}$ = 335 ± 3 GPa from the second-order fit and $K_{0T}$ = 350 ± 16 GPa with $K_{0T}'$ = 3.3 ± 0.7 from the third-order fit. All these values are summarized in Table 4.

The bulk modulus data suggest that this new superhard solid solution ($W_{0.93}Ta_{0.02}Cr_{0.05}B_4$) may be slightly stiffer than pure $WB_4$. This result is counterintuitive, since the bulk modulus


dx.doi.org/10.1021/ja308219r | J. Am. Chem. Soc. 2012, 134, 20660−20668

**Table 4. Measured Isothermal Bulk Modulus ($K_{0T}$) and Corresponding First Derivatives ($K_{0T}'$) of $WB_4$ and $W_{0.93}Ta_{0.02}Cr_{0.05}B_4$ Solid Solution Using an *in Situ* High-Pressure XRD Technique[a]**

| | $WB_4$ | | $W_{0.93}Ta_{0.02}Cr_{0.05}B_4$ | |
|---|---|---|---|---|
| pressure (GPa) | $K_{0T}$ (GPa) | $K_{0T}'$ | $K_{0T}$ (GPa) | $K_{0T}'$ |
| 40 | 326 (3) | 4 | 346 (3) | 4 |
| | 369 (9) | 1.2 (0.5) | 366 (14) | 2.6 (0.9) |
| 65 | – | – | 335 (3) | 4 |
| | – | – | 350 (16) | 3.3 (0.7) |

[a]Data were fit using the second- and third-order Birch–Murnaghan equations of state up to 40 and 65 GPa. Error values are quoted in parentheses.

usually follows Vegard's law for solid solutions,[20] and neither Ta nor Cr borides are predicted to be significantly stiffer than $WB_4$. $TaB_2$ is reported to have an experimentally determined bulk modulus value of 341 ± 7 GPa,[27] which is very similar to $WB_4$. Only theoretical values are available for $CrB_4$, but it is predicted to be much softer than $WB_4$, with a bulk modulus in the range of 265–275 GPa.[28] The observation of a small increase in bulk modulus based on the second-order fits for the ternary solid solution thus lends support to the idea that many of the mechanical changes in these materials are electronic in origin. In the case of bonding changes, one would not expect samples to follow Vegard's law. Note that in addition to $K_{0T}$, the shear modulus ($G$) also has a significant contribution to hardness.[25] $K_{0T}$ (and also $G$) can be independently constrained through ultrasonic and/or Brillouin spectroscopic measurements. This would allow for confirmation of values obtained using the third-order finite strain Birch–Murnaghan equation of state.

Further examination of the high-pressure data shows a number of other interesting trends when $W_{0.93}Ta_{0.02}Cr_{0.05}B_4$ is compared to $WB_4$. First of all, the solid solution is mechanically more isotropic than pure $WB_4$. That is, the compressibility in the $a$- and $c$-directions is more similar in $W_{0.93}Ta_{0.02}Cr_{0.05}B_4$ than they are in $WB_4$. Figure 3b shows the linear compressibility of $W_{0.93}Ta_{0.02}Cr_{0.05}B_4$ in the $a$- and $c$-directions. For $WB_4$, the $c$-direction is found to be 24% less compressible (i.e., stiffer) than the $a$-direction.[18] By contrast, Figure 3b indicates that $W_{0.93}Ta_{0.02}Cr_{0.05}B_4$ is less compressible in the $a$-axis than it is along the $c$-axis, though the difference is only 11%. It is unlikely that such a swap of the most compressible direction could stem from anything other than a change in electronic structure, again emphasizing that this very hard solid solution shows fundamentally altered bonding, compared to pure $WB_4$.

Perhaps more dramatic is the comparison shown in Figure 4, which plots the $c/a$ ratio as a function of pressure for $W_{0.93}Ta_{0.02}Cr_{0.05}B_4$ (Figure 4a) and for the parent binary solid solution $W_{0.98}Ta_{0.02}B_4$ (Figure 4b) compared with pure $WB_4$. $WB_4$ is observed to undergo a second-order phase transition at ~42 GPa, which manifests itself as a sudden change in the $c/a$ ratio.[18] In contrast, no significant changes in $c/a$ ratio are observed for the solid solutions over the same pressure range. It has been hypothesized that the softening in the $c$-direction is a structural rearrangement required to reoptimize the bonding in $WB_4$ at high levels of compression.[18] The fact that this phase transition is not observed in the solid solutions re-emphasizes that the addition of just 2 at. % Ta to $WB_4$ can create a material with significantly altered bonding.

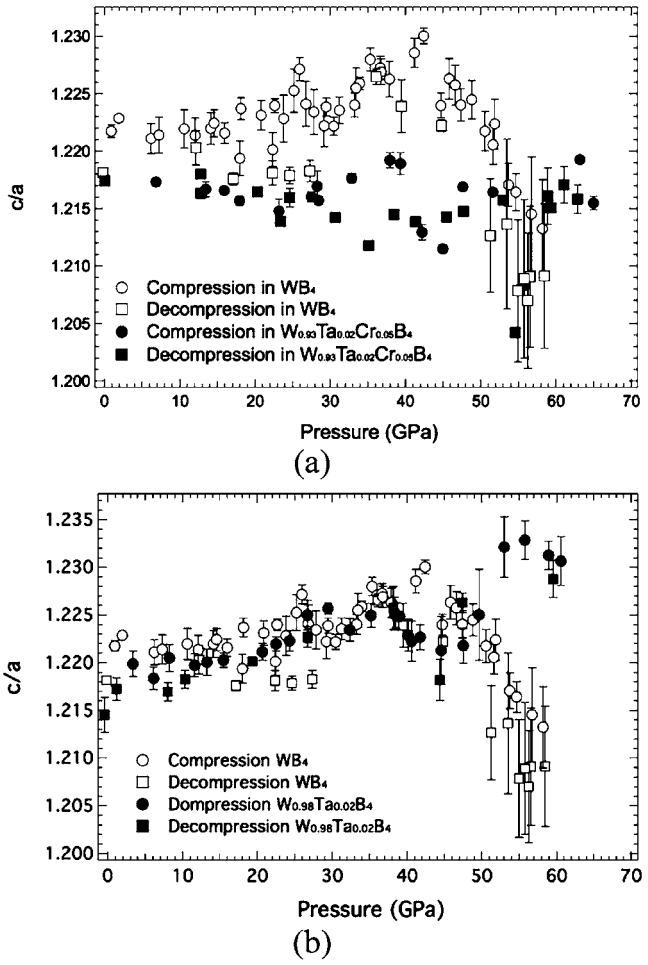


**Figure 4.** The $c/a$ ratio plotted as a function of pressure for the $W_{0.93}Ta_{0.02}Cr_{0.05}B_4$ (a) and $W_{0.98}Ta_{0.02}B_4$ (b) solid solutions compared with pure $WB_4$. Solid circle (●), compression of the solid solution; solid square (■), decompression of the solid solution; open circle(○), compression of $WB_4$; open square (□), decompression of $WB_4$. $WB_4$ undergoes a pressure-induced second-order phase transition at ~42 GPa. In contrast, $W_{0.93}Ta_{0.02}Cr_{0.05}B_4$ and $W_{0.98}Ta_{0.02}B_4$ show no evidence of a phase transition up to the highest pressure, suggesting a significant effect of W substitution on the bonding. Error bars are within the size of the symbols.

Our last test involved investigation of the thermal stability of our hardest $WB_4$ solid solution ($W_{0.93}Ta_{0.02}Cr_{0.05}B_4$) using thermal gravimetric analysis. The results (Figure 5) indicate that a powder of this solid solution is thermally stable in air up to ~420 °C, which is slightly higher than the thermal stability of pure $WB_4$ (~400 °C) measured under the same experimental conditions.[17] The final products of the thermal reaction in air consisted of $WO_3$ and $Cr_2O_3$ as determined by powder XRD. The thermal stability in air is a key figure of merit for hard materials, which are often used for cutting tools. In such applications, high-temperature oxidation can be a significant route to materials failure.

## ■ CONCLUSIONS

Compositional variations of $WB_4$ with Ta, Mn, and Cr were synthesized in an attempt to create superhard transition-metal borides with ever increasing hardness. By adding 2 at. % Ta, 4 at. % Mn, and 10 at. % Cr on a metals basis, the Vickers hardness (under an applied load of 0.49 N) of $WB_4$ increases


dx.doi.org/10.1021/ja308219r | J. Am. Chem. Soc. 2012, 134, 20660–20668

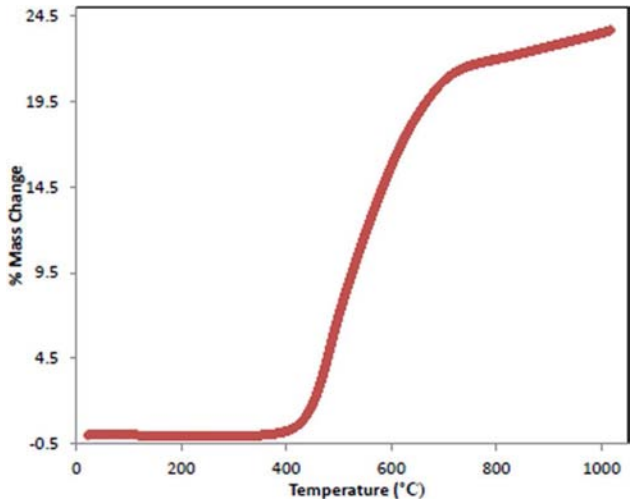


**Figure 5.** Thermal stability of the hardest tungsten tetraboride solid solution, $W_{0.93}Ta_{0.02}Cr_{0.05}B_4$, as measured by thermal gravimetric analysis. These data show that this $WB_4$ solid solution is thermally stable up to 420 °C in air. The weight gain of about 20−25% above 420 °C can be attributed to the oxidation of tungsten and chromium to $WO_3$ and $Cr_2O_3$, respectively, as determined using powder XRD.

from 43.3 to 52.8, 53.7, and 53.5 GPa for these three solid solutions, respectively. Significant increases in the concentration of any of these three transition-metal elements switch the hardness from an intrinsic regime to an extrinsic mode, resulting from dispersion hardening, which occurs at a concentration of ∼40 at. % for all three solid solution series.

In an attempt to create even harder materials, we synthesized ternary solid solutions of $WB_4$ containing all three of these transition metals by keeping the concentration of Ta constant at 2 at. % on a metals basis and changing those of Mn or Cr from 2 to 10 at. %. This resulted in the formation of the hardest $WB_4$ solid solution, $W_{0.93}Ta_{0.02}Cr_{0.05}B_4$, with a Vickers hardness of 57.3 ± 1.9 GPa (under 0.49 N). This material possesses a bulk modulus in the range of 335−366 GPa, depending on the fitting method used, as determined by *in situ* high-pressure XRD. These values are slightly higher than those obtained for pure $WB_4$. More importantly, the solid solution showed significantly altered bonding as evidenced by the absence of a second-order phase transition that was observed in $WB_4$ and more isotropic compressibility. The solid solution is also thermally stable in air up to ∼420 °C.

This work thus represents a significant step forward in the search for low-cost, easily manufactured hard materials. When $ReB_2$ was first shown to be superhard at low loads, the results were heralded as a breakthrough in hard materials. At the same time, it was clear that $ReB_2$ would be less likely to result in a practical system because of the high cost of Re. $WB_4$ is a comparatively low-cost material, and the data presented here show that it can be converted to a material with significantly higher hardness than $ReB_2$ by the addition of small amounts of relatively low-cost elements. It is our hope that theory will be able to provide a predictive understanding of the bonding changes that occur in these solid solutions and that others will build on these results to produce solid solutions with even higher hardnesses. By moving from pure phases to solid solutions, we can dramatically increase the bonding in this exciting class of hard materials. Table 5 compares the properties of $W_{0.93}Ta_{0.02}Cr_{0.05}B_4$ with other known superhard materials.

## ■ ASSOCIATED CONTENT

### Ⓢ Supporting Information

XRD data obtained for ternary solid solutions of $WB_4$ with Ta and Mn or Cr. Series of representative diffraction patterns for the hardest solid solution ($W_{0.93}Ta_{0.02}Cr_{0.05}B_4$). This material is available free of charge via the Internet at http://pubs.acs.org.

## ■ AUTHOR INFORMATION

### Corresponding Author

kaner@chem.ucla.edu; tolbert@chem.ucla.edu

### Notes

The authors declare no competing financial interest.

## ■ ACKNOWLEDGMENTS

The authors would like to thank Dr. Julio M. D'Arcy and Mr. Michael T. Yeung for their assistance with EDS and XRD experiments, respectively. We also thank Prof. Benjamin M. Wu at the UCLA Department of Bioengineering for use of his microindentation system. Financial support for this research from the National Science Foundation under grant 1106364 (S.H.T. and R.B.K.) and the Natural Science and Engineering Council of Canada (R.M.) is gratefully acknowledged. Portions of this work were performed at the Advanced Light Source, Lawrence Berkeley National Laboratory. The Advanced Light Source is supported by the Director, Office of Science and Office of Basic Energy Sciences of the U.S. Department of Energy under contract no. DE-AC02-05CH11231. Some parts

**Table 5. Vicker's Hardness ($H_v$), Isothermal Bulk Modulus ($K_{0T}$), Shear Modulus ($G$), and Young's Modulus ($E$) of Major Superhard Materials Compared to Our Hardest Solid Solution, $W_{0.93}Ta_{0.02}Cr_{0.05}B_4$**

| compound | $H_v$ (GPa) | $K_{0T}$ (GPa) | $G$ (GPa) | $E$ (GPa) |
|---|---|---|---|---|
| diamond | 60−150[15] | 433−443[15,16] | 534−535[15] | 1142[15] |
| *c*-BN | 45−80[1,15] | 369−385[1,15] | 409[15] | 800−900[1] |
| $B_6O$ | 35[15] | 200−208[15] | 204[15] | 472[29] |
| $BC_2N$ | 62−76[1] | 259[30] | 238[30] | 980[31] |
| $Si_3N_4$ | 33[15] | 249[15] | 123[15] | 280[15] |
| $Al_2O_3$ | 20−27[1,15] | 246−252[15,16] | 160−166[15] | 403−44[15] |
| *α*-SiC | 21−29[1,15] | 221−234[15] | 198−200[15] | 457−466[15] |
| *β*-SiC | 26−37[15] | 210−227[15] | 170−173[15] | 401−410[15] |
| WC | 13−25[1] | 412−421[15] | 269−280[15] | 700−720[15] |
| $ReB_2$ | 30−48[1] | 344[17] | 267−273[1,3] | 614−661[1,3] |
| $WB_4$ | 28−43[17] | 326 (this work) | 245 (theoretical)[32] | 553[17] |
| $W_{0.93}Ta_{0.02}Cr_{0.05}B_4$ | 32−57 (this work) | 335 (this work) | – | – |

of this study were carried out at GeoSoilEnviroCARS (Sector 13), Advanced Photon Source (APS), Argonne National Laboratory. GeoSoilEnviroCARS is supported by the National Science Foundation−Earth Sciences (EAR-0622171) and Department of Energy−Geosciences (DE-FG02-94ER14466). APS is supported by DOE-BES, under contract no. DE-AC02-06CH11357. This research was partially supported by the Consortium for Materials Properties Research in Earth Sciences (COMPRES) under NSF Cooperative Agreement EAR 11-57758.

## REFERENCES

(1) Mohammadi, R.; Kaner, R. B. Superhard Materials. In *Encyclopedia of Inorganic and Bioinorganic Chemistry*; Scott, R. A., Ed.; John Wiley: Chichester, 2012.
(2) Kaner, R. B.; Gilman, J. J.; Tolbert, S. H. *Science* **2005**, *308*, 1268−1269.
(3) Levine, J. B.; Tolbert, S. H.; Kaner, R. B. *Adv. Funct. Mate.r.* **2009**, *19*, 3519−3533.
(4) Chung, H. Y.; Weinberger, M. B.; Levine, J. B.; Kavner, A.; Yang, J. M.; Tolbert, S. H.; Kaner, R. B. *Science* **2007**, *316*, 436−439.
(5) Levine, J. B.; Nguyen, S. L.; Rasool, H. I.; Wright, J. A.; Brown, S. E.; Kaner, R. B. *J. Am. Chem. Soc.* **2008**, *130*, 16953−16958.
(6) Tkachev, S. N.; Levine, J. B.; Kisliuk, A.; Sokolov, A. P.; Guo, S. Q.; Eng, J. T.; Kaner, R. B. *Adv. Mater.* **2009**, *21*, 4284−4286.
(7) Levine, J. B.; Betts, J. B.; Garrett, J. D.; Guo, S. Q.; Eng, J. T.; Migliori, A.; Kaner, R. B. *Acta Mater.* **2010**, *58*, 1530−1535.
(8) Suzuki, Y.; Levine, J. B.; Migliori, A.; Garrett, J. D.; Kaner, R. B.; Fanelli, V. R.; Betts, J. B. *J.Acoust. Soc. Am.* **2010**, *127*, 2797−2801.
(9) Cumberland, R. W.; Weinberger, M. B.; Gilman, J. J.; Clark, S. M.; Tolbert, S. H.; Kaner, R. *J. Am. Chem. Soc.* **2005**, *127*, 7264−7265.
(10) Chung, H. Y.; Yang, J. M.; Tolbert, S. H.; Kaner, R. B. *J. Mater. Res.* **2008**, *23*, 1797−1801.
(11) Romans, P. A.; Krug, M. P. *Acta Crystallogr.* **1966**, *20*, 313−315.
(12) Itoh, H.; Matsudaira, T.; Naka, S.; Hamamoto, H.; Obayashi, M. *J. Mater. Sci.* **1987**, *22*, 2811−2815.
(13) Liu, C.; Peng, F.; Tan, N.; Liu, J.; Li, F.; Qin, J.; Wang, J.; Wang, Q.; He, D. *High Pressure Res.* **2011**, *31*, 275−282.
(14) Rau, J. V.; Latini, A.; Teghil, R.; De Bonis, A.; Fosca, M.; Caminiti, R.; Albertini, V. R. *ACS Appl. Mater. Interfaces* **2011**, *3*, 3738−3743.
(15) Brazhkin, V. V.; Lyapin, A. G.; Hemley, R. J. *Philos. Mag.* **2002**, *82*, 231−253.
(16) Gu, Q.; Krauss, G.; Steurer, W. *Adv. Mater.* **2008**, *20*, 3620−3626.
(17) Mohammadi, R.; Lech, A. T.; Xie, M.; Weaver, B. E.; Yeung, M. T.; Tolbert., S.; Kaner, H.; Tungsten Tetraboride, R. B. *P. Natl. Acad. Sci. U.S.A.* **2011**, *108*, 10958−10962.
(18) Xie, M.; Mohammadi, R.; Zhu, M.; Armentrout, M. M.; Kavner, A.; Kaner, R. B.; Tolbert, S. H. *Phys. Rev. B* **2012**, *85*, 064118(8 pp).
(19) Dieter, G. E. *Mechanical Metallurgy*; McGraw Hill: New York, 1986.
(20) Weinberger, M. B.; Levine, J. B.; Chung, H. Y.; Cumberland, R. W.; Rasool, H.; Yang, J. M.; Kaner, R. B.; Tolbert, S. H. *Chem. Mater.* **2009**, *21*, 1915−1921.
(21) Egami, T.; Waseda, Y. *J. Non-Cryst. Solids* **1984**, *64*, 113−134.
(22) Revers, M.; Prakapenka, V. B.; Kubo, A.; Pullins, C.; Holl, C. M.; Jacobsen, S. D. *High Press. Res.* **2008**, *28*, 273−292.
(23) Wang, M.; Li, Y. W.; Cui, T.; Ma, Y. M.; Zou, G. T. *Appl. Phys. Lett.* **2008**, *93*, 101905 (3 pp).
(24) Gou, H.; Li, Z.; Wang, L. M.; Lian, J.; Wang, Y. *API Adv.* **2012**, *2*, 012171 (9 pp).
(25) Teter, D. M. *MRS Bull.* **1998**, *23*, 22−27.
(26) Veprek, S. *J. Vac. Sci. Technol. A* **1999**, *17*, 2401−2420.
(27) Winkler, B.; Juarez-Arellano, E. A.; Friedrich, A.; Bayarjargal, L.; Schröder, F.; Biehler, J.; Milman, V.; Clark, S. M.; Yan, J. *Solid State Sci.* **2010**, *12*, 2055−2064.
(28) Gou, H.; Li, Z.; Niu, H.; Gao, F.; Zhang, J.; Ewing, R. C.; Lian, J. *Appl. Phys. Lett.* **2012**, *100*, 111907 (4 pp).
(29) Lu, Y. P.; He, D. W. *J. App. Phys.* **2009**, *105*, 083540 (7 pp).
(30) Tkachev, S. N.; Solozhenko, V. L.; Zinin, P. V.; Manghnani, M. H.; Ming, L. C. *Phys. Rev. B* **2003**, *68*, 052104 (3 pp).
(31) Solozhenko, V. L.; Dub, S. N.; Novikov, N. V. *Diam. Relat. Mater.* **2001**, *10*, 2228−2231.
(32) Zhang, R. F.; Legut, Z. D.; Lin, J.; Zhao, Y. S.; Mao, H. K.; Veprek, S. *Phy. Rev. Lett.* **2012**, *108*, 255502 (5 pp).